Materials Science and Engineering B 159–160 (2009) 318–321

Contents lists available at ScienceDirect

Materials Science and Engineering B

journal homepage: www.elsevier.com/locate/mseb

Influence of metal grid patterns on the performance of silicon solar cells at different illumination levels

P. Morvillo*, E. Bobeico, F. Formisano, F. Roca

ENEA, C.R. Portici, Loc. Granatello, 80055 Portici (NA), Italy

ARTICLE INFO

Article history:
Received 2 May 2008
Received in revised form
18 September 2008
Accepted 9 October 2008

Keywords:
Silicon
Solar cell
Concentration
Metal grid
Simulation

ABSTRACT

In the present work we have investigated, both theoretically and experimentally, the effect of two different metal grid patterns, one with 2 busbars outside the active area (linear grid) and another one with a square busbar surrounding the active area (square grid) on the electrical performance of high efficiency c-Si solar cells under concentrated light (up to 200 suns). We calculated the power losses of both grid patterns at different illumination levels. We found that the power losses of the square grid are less sensitive to illumination levels compared to linear grid; this is true especially under medium and high concentration ratio. Moreover, the power losses of the square grid are also less influenced by metal grid resistivity. We fabricated and characterized also a large number of c-Si solar cells (more than 100 for each grid design) to prove the theoretical findings.

1. Introduction

Although the development of solar power engineering is very intensive, actually the cost of this kind of energy is still higher than that obtained from conventional sources. Photovoltaic concentrators have a high potential to achieve cost reduction for solar-generated electricity [1,2]. Different studies indicate that energy production cost of photovoltaic concentrators can occur at a fraction of the energy production costs of module plants in countries having high direct solar irradiation over the year.

This cost reduction is achieved by an area reduction of highly efficient and quite expensive solar cells using cheap optical elements concentrating the light [3,4]. The fraction of the solar cell cost of the concentrator system decreases with increasing concentration factor, while the fraction of the optical elements costs and the tracking system increase. A tracking system is needed in order to collect the direct sunlight using optical elements.

Over the last 20 years the developed concentrator systems use either reflecting or refracting cheap optical elements in order to concentrate light onto the solar cells. Middle scaled concentrator power plants in the range of some 100 kW peak were built up in order to demonstrate the long time stability and reliability of concentrator systems. A detailed overview of the most important basic concentrator concepts all over the world is given in [5].

To work properly under concentrated sunlight solar cells have to be optimized, since the series resistance of the device limits the conversion efficiency at high illumination levels. The influence of series resistance has been intensively investigated by several authors [2,6–10]. One way to reduce the resistance is to increase the grid coverage, but at the expense of blocking light from the cell. An optimum grid-line pattern minimizes the combined effect of the four loss mechanisms directly associated with the grid. They are: (1) emitter-layer resistance; (2) grid-metal resistance; (3) shading loss due to grid reflection; (4) contact resistance between the metal and the semiconductor. Other loss mechanisms in the cell typically have little or no dependence on the pattern selected for the front-surface grid, and thus, usually, are not included into the analysis [11,12].

Generally, during the design of the metal grid of a solar cell the width of the metal fingers is fixed by technological constraints. The optimization of the metal grid is practically restricted to finding the separation between the fingers that results in the best compromise among shading and resistive losses.

Although in the literature it is possible to find various papers that model the influence of different contacting grid patterns on the performance of a solar cell under concentrating light [13–16], the experimental demonstrations are rare.

In the present work we have investigated, both theoretically and experimentally, the influence of two different metal grid patterns on the electrical performance of high efficiency silicon solar cells

* Corresponding author at: ENEA, C.R. Portici, Loc. Granatello, I-80055 Portici (NA), Italy. Tel.: +39 0817723260; fax: +39 0817723345.
E-mail address: morvillo@portici.enea.it (P. Morvillo).

0921-5107/$ – see front matter © 2008 Elsevier B.V. All rights reserved.
doi:10.1016/j.mseb.2008.10.004

at one sun and under concentrated light (up to 200 suns). We have analyzed also the effect of the metal finger resistivity on the power losses of the grid at different illumination levels. A conventional solar cell structure has been used and more than 100 devices for each kind of metal grid pattern have been realized and tested to confirm the theoretical findings.

2. Device simulation

The simulation of the c-Si solar cell has been made by PC1D computer program [17] which solves the fully coupled nonlinear equations for the quasi-one-dimensional transport of electrons and holes in crystalline semiconductor device. The program allows the user to specify all necessary parameters which determine device performance. Using PC1D, we simulated the efficiency of our cell at one sun and under concentrated light (till 200 suns) taking in account the experimental reflectance of our antireflection layer and the doping profile determined by SRP (spread resistance profile); the program does not consider frontal metal grid losses.

We have investigated 2 different top contact grid structures: the first one with two busbars outside the active area of the device (linear grid, Fig. 1a) and the second one with four busbars surrounding the active area (square grid, Fig. 1b). For both geometries, the fingers are considered uniform and equally spaced.

For each finger, the power losses caused by each component of the series resistance (emitter resistance (Eq. (1)), contact resistance (Eq. (2)), metal resistance (Eq. (3))) and by the shadowing (Eq. (4)) were calculated using the simple model reported in Refs. [11,12]:

$$p_e = \frac{R_e J_{mp}}{12 V_{mp}} S^2 \quad (1)$$

$$p_m = \frac{1}{12} L^2 R_m \frac{J_{mp}}{V_{mp}} \frac{S}{W_F} \quad (2)$$

$$p_c = \rho_c \frac{J_{mp}}{V_{mp}} \frac{S}{W_F} \quad (3)$$

$$p_s = \frac{W_F}{S} \quad (4)$$

where p_e is the loss due to the lateral current flow in the top diffused layer, p_m is the loss due to the series resistance of the metal lines, p_c is the loss due to the contact resistance between these lines and the semiconductor, p_s is the loss due to the grid shadowing, R_m is the sheet resistance of the metal fingers, R_e is the sheet resistance of the emitter layer, ρ_c is the specific contact resistance, S is the distance between two adjacent fingers, L and W_F are the finger length and width, respectively, and J_{mp} and V_{mp} are the current density and voltage, respectively, at the maximum power output.

The power losses of the whole grid was calculated summing the power losses of each grid finger weighed with the finger length. Because the grid finger width limit of our photolithographic process is around 20 μm (for a finger height of 10 μm), the optimization of the metal grid was practically restricted to finding the separation between the fingers that results in the best compromise between shading and resistive losses. The grid spacing was optimized to minimize the power losses of the grid under a concentration of 150 suns.

3. Experimental part

In our process we have used monocrystalline ⟨1 0 0⟩ oriented silicon floating zone 250 μm thick wafers having high p-type doping density as well as 0.1 Ω cm resistivity. Our photolithographic mask allows to obtain on a single 4 in. silicon wafer 30 cells (the active area of each device is 1.21 cm^2 with an external busbar having a width of 0.5 mm).

The experimental steps of the cells fabrication are summarized below. After standard RCA cleaning procedure the n-type emitter is realized on the top of the wafer by a diffusion process at 850 °C starting from a $POCl_3$ source. The remaining SiO_2–P_2O_5 is removed by a wet chemical etching in 5% HF bath. SRP profiles have been carried out on the n–p junction to optimize the doping distribution. To reduce surface recombination velocity, a 18-nm thick thermal oxide is grown at 850 °C. The back contact of the cell is realized by e-beam evaporation of 2 μm Al layer annealed at 550 °C. The front contact is ensured by an e-beam evaporation of a trilayer of Ti, Pd, Ag (10 μm) on which a grid for the impinging light is obtained by lift-off process. A 6 μm deep trench is formed by a wet chemical etch around the perimeter of the cell. A double antireflection coating (DARC) of ZnS and MgF_2 evaporated on the top of the device has been optimized to reduce the total reflectance below 8%.

All the solar cells have been characterized by external quantum efficiency and current–voltage measurements performed in dark and light range from 1 to 200 suns using a flashed simulator (Pasan Sun Simulator III) with a pulsed xenon lamp (AM 1.5 D spectral distribution and 1000 W/m^2 irradiance). Light has been concentrated using a Fresnel lens. All the measurements were carried out at 25 °C. The input irradiance is calculated by assuming that the short circuit current density (Jsc) of the cell is linear with respect to the irradiance. The concentration ratio is thus the ratio of the Jsc under concentration and the Jsc at one sun [18].

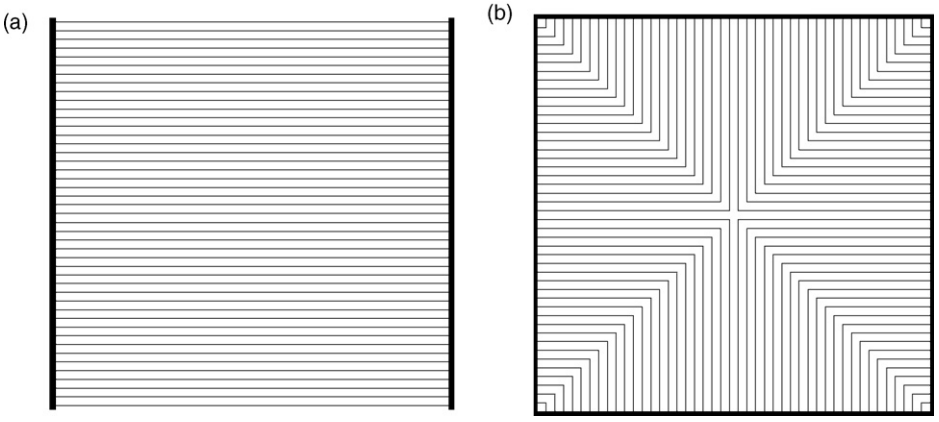

Fig. 1. The investigated top contact grid patterns: linear grid (a) and square grid (b).

4. Discussion

4.1. Metal grid losses

We calculated the power losses of both grid patterns at one sun and under concentrated light considering for both grids the same finger spacing (244.4 μm) obtained minimizing the power losses of the square grid at 150 suns. Although the optimized finger spacing for the linear grid is slightly less, we preferred to consider the same value of the square grid because in this case the shadowing losses are equal for both geometries and all the differences are due to losses arising from resistances of the contacting structure (emitter, contact and metal resistance). Moreover, the losses of the linear grid with the optimized finger spacing (at 150 suns) are very close to the ones calculated using the previous value (differences less than 0.3%).

Under concentrating light, the square grid has less power losses compared to the linear grid mainly because the average length of the fingers is half than the one of the linear grid and the power losses due to metal resistivity are reduced.

We also calculated the power losses at different concentrations for 3 values of metal resistivity ($4 \times 10^{-6}\ \Omega$ cm, $8 \times 10^{-6}\ \Omega$ cm and $1.2 \times 10^{-5}\ \Omega$ cm). The resistivity of the evaporated (thin film) metal fingers is greater compared to the bulk value [15]; for this reason it is important to take in account also this variable. As we can see from Fig. 2 the losses of the square grid is always less compared to the one of the linear grid. For low concentration ratios the difference is very small but it increases dramatically with the concentration. Although the power losses of a grid pattern increase with metal finger resistivity, as expected, the square grid is less sensitive to this variation.

4.2. Experimental results

We made a comparative study of the electrical behaviour of different devices (current–voltage and quantum efficiency characterization) at one sun and under concentrated light (up to 200 suns), to investigate the influence of the two metal grid patterns on the electrical performances of the devices. The feasibility of the devices is proven by the fabrication of a number of cells with similar performances (more than 100 for each metal grid investigated). The best cell realized in our laboratory (using the square grid), reached the efficiency of 22% at 100 suns and more than 20% at 200 suns.

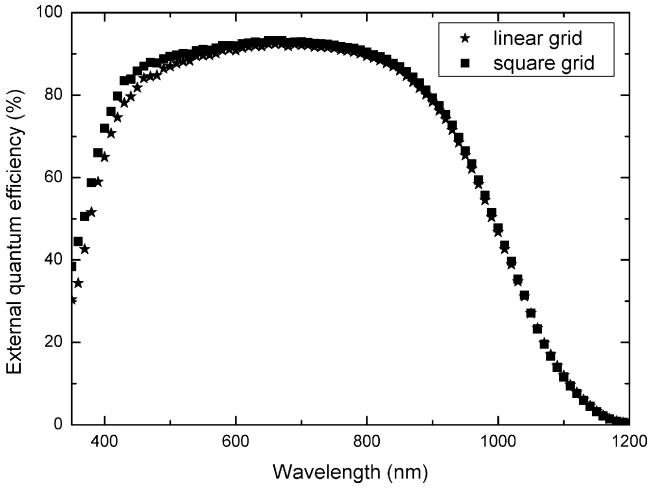

Fig. 3. External quantum efficiency for c-Si solar cells realized with the linear and square grid.

Below we focus our discussion only on the average electrical parameters obtained for the cells realized with the 2 investigated grids.

The shadowing losses of both grids are equal and the Jsc for the corresponding devices is similar as we can see from Fig. 3, where the external quantum efficiencies for both devices are compared.

In Fig. 4 we report the average open circuit voltage (Voc) at different illumination levels for the devices realized with the 2 kinds of grid patterns. As we can see, the linear grid has higher values than the one of square grid for all the concentration range. This behaviour is not anomalous. Although the active area for both metal grid pattern is equal, we have to remark that the surface covered by the busbars is greater for the square grid because there is a square busbar surrounding the active area of the device. In our process the busbar is not isolated from the semiconductor material and for this reason we can expect an increased recombination at the metal–silicon interface. This can raise the value of the saturation current that influences the Voc. The Voc is proportional to the logarithm of the ratio between the light generated current and the saturation current (i.e. if the saturation current increases, the Voc decreases). We confirmed that the saturation current for devices prepared with the square grid is greater than the one for devices

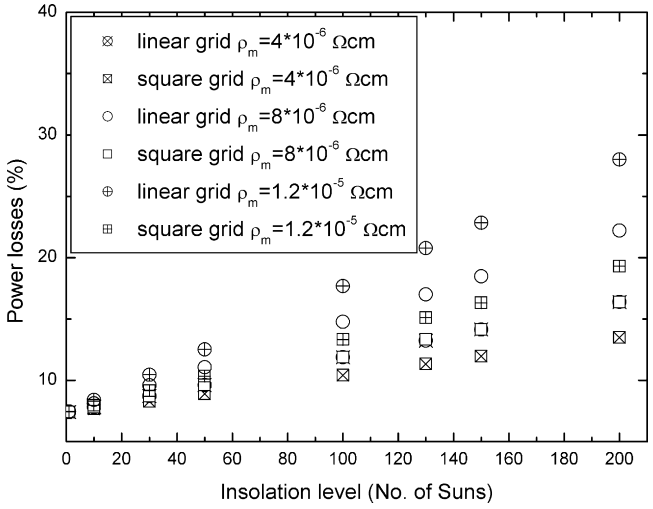

Fig. 2. The calculated power losses at different illumination levels for the linear and the square grid.

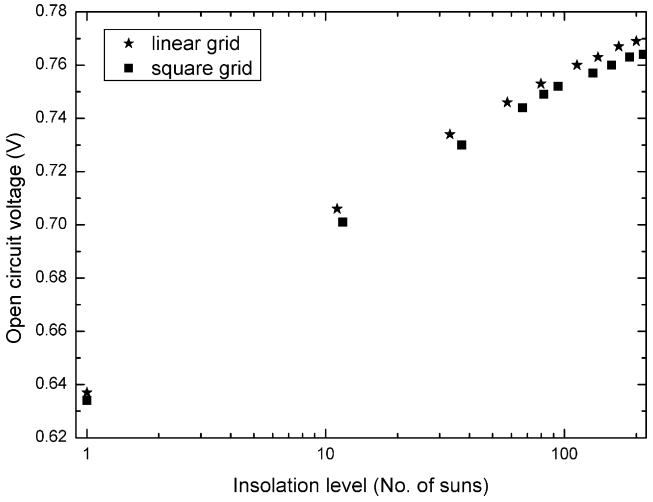

Fig. 4. Average open circuit voltage at different illumination levels for c-Si solar cells realized with the linear and square grid.

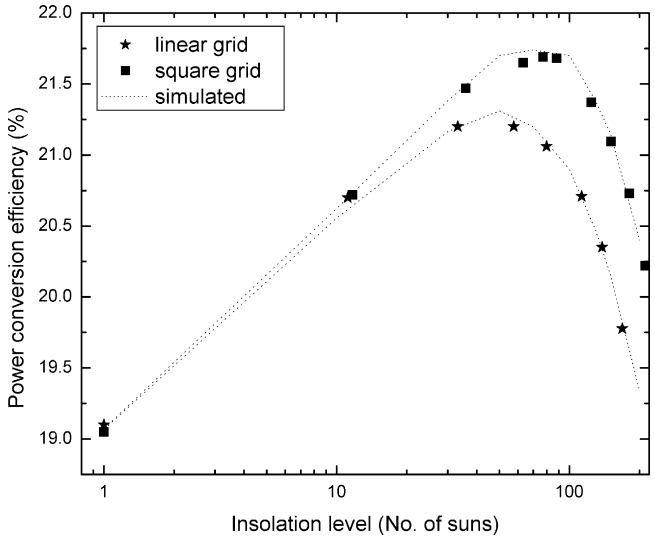

Fig. 5. Average power conversion efficiency at different illumination levels for c-Si solar cells realized with the linear and square grid. The simulated efficiencies (dotted lines) are also reported.

with linear grid, deriving the saturation current from the IV dark measurements.

In Fig. 5 we show the average power conversion efficiency under concentrated light for the devices realized with the linear and the square grid; we report also the theoretical performance for these cells calculated correcting the efficiency of our device determined with PC1D with the power losses of the two metal grids. The performance of the cells realized with the square grid overcome the one of the cells realized with the linear grid. Moreover, the maximum of the efficiency is shifted to higher concentration values.

Although the square grid show less power losses compared to linear grid, we have to remark that c-Si solar cells for concentrating systems often are fabricated with a linear grid, reducing the potential performances of the device. We have shown that also using a simple device structure, the decrease in efficiency is around 1.5% at 100 suns.

5. Conclusions

In this work we have investigated, both theoretically and experimentally, the effect of two different metal grid patterns (one with 2 busbars and another one with a square busbar surrounding the active area) on the electrical performance of high efficiency c-Si solar cell under concentrated light. We found that the power losses of the square grid are less sensitive to illumination levels compared to linear grid; this is true especially under medium and high concentration ratio. Moreover, the power losses of the square grid are also less influenced by metal grid resistivity.

References

[1] R.M. Swanson, Prog. Photovolt.: Res. Appl. 8 (2000) 93–111.
[2] A. Luque, Bristol (1989).
[3] R.M. Swanson, Proc. 19th Europ. Photovolt. Solar Energy Conference, Paris, France, 2004 pp. 1078–1081.
[4] H.J. Moller, Solid State Phenom. 47–48 (1996) 127–142.
[5] R.M. Swanson, in: A. Luque, S. Hegedus (Eds.), Handbook of Photovoltaic Science and Engineering, John Wiley & Sons, Ltd., 2003.
[6] G.L. Araujo, A. Cuevas, J.M. Ruiz, IEEE Trans. Electron Devices 33 (1986) 391–401.
[7] M. Wolf, H. Rauschenbach, Adv. Energy Conv. 3 (1963) 455–479.
[8] A. de Vos, Sol. Cells 12 (1984) 311–327.
[9] A.G. Aberle, S.R. Wenham, M.A Green, Conf. Rec. 23rd IEEE Photovoltaic Spec. Conf., IEEE, Piscataway, New York, 1993 pp. 133–139.
[10] C. Algora, V. Diaz, Prog. Photovolt.: Res. Appl. 8 (2000) 211–225.
[11] M.A. Green, Solar Cells: Operating Principles Technology and System Applications, University of New South Wales, Sydney, 1995.
[12] A. Cuevas, D. Russel, Prog. Photovolt.: Res. Appl. 8 (2000) 603–616.
[13] P.A. Basore, Sol. Cells 14 (1985) 249–260.
[14] A. Antonini, M. Stefancich, D. Vincenzi, C. Malagù, F. Bizzi, A. Ronzoni, G. Martinelli, Sol. Energy Mater. Sol. Cells 80 (2003) 155–166.
[15] T.A. Gessert, T.J. Coutts, J. Vac. Sci. Technol. A 10 (1992) 2013–2024.
[16] A.R. Burgers, Prog. Photovolt.: Res. Appl. 7 (1999) 457–461.
[17] D.A. Clugston, P.A. Basore, PC1D Version 5:32-bit Solar Cell Simulation on Personal Computers 26th IEEE Photovoltaic Specialists Conf., September, 1997.
[18] J.M. Gee, B.R. Hansen, Sol. Cells 18 (1986) 281–288.